FISEVIER

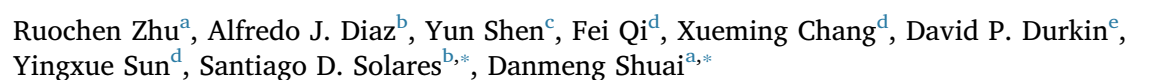
Contents lists available at ScienceDirect

## Journal of Membrane Science

journal homepage: www.elsevier.com/locate/memsci



## Mechanism of humic acid fouling in a photocatalytic membrane system





- <sup>a</sup> Department of Civil and Environmental Engineering, The George Washington University, Washington D.C. 20052, United States
- <sup>b</sup> Department of Mechanical and Aerospace Engineering, The George Washington University, Washington D.C. 20052, United States
- <sup>c</sup> Department of Civil and Environmental Engineering, University of Michigan, Ann Arbor, MI 48109, United States
- <sup>d</sup> Department of Environmental Science and Engineering, Beijing Technology and Business University, Beijing 100048, China
- e Department of Chemistry, United States Naval Academy, Annapolis, MD 21402, United States

#### ARTICLE INFO

#### Keywords: Humic acid Photocatalysis Ultrafiltration membrane Adhesion force Fouling mechanism

#### ABSTRACT

Photocatalytic membrane filtration has emerged as a promising technology for water purification because it integrates both physical rejection and chemical destruction of contaminants in a single unit, and also largely mitigates membrane fouling by natural organic matter (NOM). In this study, we evaluated the performance of a photocatalytic membrane system for mitigating fouling by a humic acid, which is representative NOM, and identified critical properties of the humic acid that determined membrane fouling. We prepared a partially oxidized humic acid (OHA) through the photocatalysis of a purified humic acid (PHA), and the OHA showed reduced fouling for polyvinylidene fluoride (PVDF) ultrafiltration membranes compared to PHA. Molecular-level characterizations indicated that OHA had a reduced molecular size, an increased oxygen content, and increased hydrophilicity. OHA also formed smaller aggregates on the fouled membrane surfaces than PHA. The introduction of oxygen-containing, hydrophilic functional groups, e.g., -OH and -COOH, to the humic acid and the depolymerization or mineralization of the humic acid in photocatalysis could result in the reduction of the foulant-membrane and foulant-foulant interactions, as characterized by atomic force microscopy (AFM), thereby mitigating membrane fouling. Foulant-membrane adhesion forces were always larger than foulant-foulant adhesion forces in our study, irrespective of the humic acid before or after photocatalytic oxidation, which may suggest that the reduction of foulant-membrane interactions is critical for membrane fouling control. In summary, this study sheds light into humic acid fouling in a photocatalytic membrane system through a systematic and comprehensive research approach, and provides insights for the design of novel membrane materials and processes with improved performance for water purification.

### 1. Introduction

Pressure-driven membrane filtration, including microfiltration, ultrafiltration, nanofiltration, and reverse osmosis, is becoming a promising physical process for the removal of a broad range of contaminants in water and wastewater [1–4]. Despite the effectiveness of membrane filtration for water and wastewater treatment, this developing technology still faces great challenges of membrane fouling, intensive chemicals and energy consumption for operation and maintenance, and further treatment or disposal of concentrated waste. Specifically, membrane fouling compromises the yield of purified water (i.e., flux), and also impairs membrane selectivity for contaminant removal [5–7]. Natural organic matter (NOM), such as humic acids, fulvic acids, and tannic acids, is ubiquitously present in various waters and

results in significant membrane fouling [8]. NOM not only accumulates on membrane surfaces or inside membrane pores to foul the membranes but also leads to the formation of disinfection byproducts (e.g., trihalomethanes, haloacetic acids) [9], and thus requires removal in water and wastewater treatment.

Many previous studies have been conducted to understand membrane fouling with NOM, by evaluating the topography of foulants on membrane surfaces, and by exploring the effect of water matrices (e.g., pH, cations), molecular sizes of the foulants, and interactions between the foulants and the membrane surfaces (e.g., electrostatic forces, hydrophobic attraction) on fouling [10–16]. To mitigate membrane fouling, different strategies have been used in engineering practices, including pre-treatment of water prior to membrane filtration (e.g., coagulation, activated carbon adsorption, oxidation), regular

E-mail addresses: ssolares@gwu.edu (S.D. Solares), danmengshuai@gwu.edu (D. Shuai).

URLS: http://solaresspmlab.com/ (S.D. Solares), http://materwatersus.weebly.com/ (D. Shuai).

<sup>\*</sup> Corresponding authors.

maintenance and cleaning of membranes (e.g., physical vibration and backwashing, chemical treatment) [17], surface modification of conventional membranes (e.g., grafting of hydrophilic and zwitterionic functional groups) [18–20]), and the development of new membranes [20]. Notably, the pre-treatment of oxidation has been demonstrated to achieve significant improvement for the removal of humic substances and to mitigate membrane fouling [21]. Taking ozonation as an example, ozone decomposes foulants into small molecules and remarkably prevents membrane fouling, due to the formation of highly reactive hydroxyl radicals (•OH) and other radicals [22,23]. However, chemical corrosion, potential toxicity, and the relatively high cost and energy consumption of the operation have prevented ozone from broad application in water purification [24,25].

Photocatalytic membrane filtration has recently emerged as a promising technology for water and wastewater treatment, and the synergy between physical separation and chemical oxidation promotes contaminant removal and mitigates membrane fouling. Photocatalysts, either suspended in water or immobilized on the membrane surfaces, produce a series of reactive oxygen species (ROS) under light illumination. The ROS can destroy small-molecule contaminants, decompose large-molecule NOM, and inactive microorganisms in water, and the process can minimize further treatment or disposal of the brine and largely mitigate membrane fouling from NOM and biofilms [26]. In addition, photocatalysts can potentially harvest sunlight and activate  $O_2$  and  $H_2O$  in ambient conditions, and thus photocatalysis can reduce the energetic and chemical footprint for water and wastewater treatment [27–29].

Our study aims to provide a molecular-level understanding of how photocatalytic membranes prevent NOM fouling in water and wastewater treatment. In this study, photocatalysts containing titanium dioxide (TiO<sub>2</sub>) were suspended in water containing a humic acid, which is typical NOM, to simulate the tandem photocatalytic membrane system of a photocatalytic slurry reactor with a downstream ultrafiltration membrane separation unit. This tandem photocatalytic membrane system was selected, in contrast to an integrated system with the photocatalyst loaded on the membrane, because the system (i) avoids polymeric membrane oxidation and deterioration in photocatalysis, (ii) improves the mass transfer rate and photoreactivity for oxidation; and (iii) allows easy illumination for photocatalysis [30-32]. TiO2 was selected because it is an inexpensive, stable, and efficient photocatalyst for water purification, and it mainly produces the most powerful oxidant •OH that reacts with most organics near diffusion-limited rates in water for NOM decomposition [33-35]. TiO<sub>2</sub> has been demonstrated to facilitate the photocatalytic oxidation of humic acids in recent years [36-39]. Uyguner et al. studied the molecular weight distribution of a humic acid after TiO2-based photocatalysis under UVA irradiation, whereby lower molecular size (less than 10 kDa) and higher UV absorbing compounds were formed [40]. Liu et al. also investigated the photocatalytic oxidation of a humic acid on TiO2, and the very hydrophobic acid fraction in the humic acid decayed rapidly to form hydrophilic charged species, whereas the hydrophilic neutral fraction was the most persistent [41]. However, due to the complex structure of humic acids and varying experimental conditions, the mechanism of photocatalytic oxidation for humic acid decomposition and consequent impacts on membrane fouling are still not well understood. How photocatalysis changes the molecular structure of the humic acids and the corresponding mechanical interactions with the membranes, which is critical for fouling mitigation, remains elusive. Moreover, previous research that compared membrane fouling mitigation before and after foulant oxidation could be misleading. Oxidation may not only tailor the molecular structure but also reduce the mass of the foulants (e.g., through mineralization), and foulant mass reduction could lead to artifacts in evaluating the effect of humic acid structural changes on membrane fouling.

Our study uses a thorough and systematic approach to understand the molecular structure of the humic acid before and after

photocatalysis, and to identify key foulant properties that determine membrane fouling. First, a commercially available humic acid was purified via acid precipitation and dialysis to obtain the purified humic acid (PHA). The PHA was then subjected to photodegradation in the presence of TiO2 to produce the oxidized humic acid (OHA) with half decay of the chemical oxygen demand (COD) as a representative photooxidized product of PHA. Next, both PHA and OHA, of the same concentration, were used to understand their fouling behaviors on an ultrafiltration membrane. The membrane flux was recorded, and physical and chemical properties of the foulants and fouled membranes were characterized by X-ray photoelectron spectroscopy (XPS), size-exclusion chromatography (SEC), fluorescence excitation-emission matrix (EEM) spectroscopy, and contact angle analysis. Atomic force microscopy (AFM) was also applied to investigate membrane fouling by the foulants at the microscale or nanoscale in an aqueous environment. AFM not only provides details of foulant topography on membrane surfaces, but also interrogates foulant and membrane mechanical properties and interactions (e.g., foulant-foulant and foulant-membrane forces, elasticity, viscosity) [42-45]. We are the first to report molecular features of the humic acid before and after photocatalytic oxidation, and the results shed light on fouling mitigation in a photocatalytic membrane system. The PHA decomposed into smaller and more hydrophilic fragments after photocatalytic oxidation, and the OHA became softer, and less adhesive to the membrane surfaces as well as to the foulant itself. This discovery can also be translated into deeper understanding of other strategies for mitigating membrane fouling (e.g., ozonation, which is currently used in industrial practices for water and wastewater treatment), and can help achieve efficient, robust, and energy- and cost-effective membrane filtration.

#### 2. Materials and methods

#### 2.1. Chemicals and materials

## 2.1.1. Chemicals

Unless otherwise specified, all chemicals were reagent grade. Milli-Q deionized water was supplied from a DIRECT-Q 3 ultrapure water purification system with a resistivity of  $18.2\,\mathrm{M}\Omega\text{-cm}$  at  $25\,^\circ\mathrm{C}$ . Sodium hydroxide (NaOH), hydrochloric acid (HCl), isopropyl alcohol, ethanol, sodium phosphate monobasic (NaH2PO4·2H2O), sodium phosphate dibasic (Na2HPO4·12H2O), sodium sulfate (Na2SO4), and TiO2 nanopowder (Aeroxide® P25, with a reported average particle size of  $21\,\mathrm{nm}$ ) were purchased from Sigma-Aldrich. A humic acid sodium salt was also purchased from Sigma-Aldrich (H16752, technical grade). Ultrafiltration membranes (YMBY3001, supplied by Synder Filtration, polyvinylidene fluoride (PVDF), molecular weight cutoff (MWCO) of  $100\,\mathrm{kDa}$ ) were purchased from Sterlitech.

#### 2.1.2. Production of purified humic acid (PHA)

The humic acid from Sigma-Aldrich was treated to remove impurities, including fulvic acids, metals, and ash, based on a modified acid and base washing method [46,47]. HCl was first added to the humic acid to produce a final concentration of 0.1 g of the humic acid per mL of the solution (ca. pH 1). The suspension was mixed for 2 h, and centrifuged at 3000 rpm for 30 min. Following the centrifugation, the supernatant was discarded, and the precipitate was re-suspended in a HCl solution (1 mol L<sup>-1</sup>). This centrifugation and resuspension procedure was repeated five times. Next, the precipitate from centrifugation was dissolved in a NaOH solution, with ca. pH 13, and the solution was mixed for 2 h and centrifuged at 3000 rpm for 30 min. The supernatant was filtered twice through 0.45 µm PVDF filters, and the filtrate was acidified to ca. pH 1.0 with HCl. After settlement over 12 h, the solution was centrifuged again at 3000 rpm for 30 min, and the precipitate was dialyzed with Spurr 7 dialysis membranes (VWR 25223-050, MWCO of 1000 Da) and freeze-dried. A stock PHA solution of  $250\,\mathrm{mg}\,\mathrm{L}^{-1}$  was prepared from the freeze-dried PHA (pH 7) and stored in the dark at

4 °C.

## 2.1.3. Production of oxidized humic acid (OHA) via photocatalysis

Photocatalytic degradation of PHA on TiO2 was used to produce OHA. The photocatalytic experiments were conducted in a temperature-controlled reactor (25 °C) under the illumination of a 1000 W Xenon lamp (Newport) with a 305 nm long-pass optical filter  $(\lambda > 305 \, \text{nm})$ . TiO<sub>2</sub> (loading of 1 g L<sup>-1</sup>) was suspended in a PHA solution (160 mg  $L^{-1}$ , equivalent to 210 mg  $L^{-1}$  as COD, 40 mL, pH 7) by continuous mixing at 500 rpm. Prior to irradiation, the reaction solution was stirred in the dark for 15 min to allow adsorption equilibrium of PHA on TiO<sub>2</sub>. During the first batch of photocatalytic reactions.  $650\,\mu L$  of the suspension was collected at different time intervals and centrifuged at 13,000 rpm, and the supernatant was analyzed for COD to determine the reaction time when half of the PHA had degraded  $(105 \,\mathrm{mg}\,\mathrm{L}^{-1})$  as COD after 4.28 h of photocatalytic degradation). The product of the photo-oxidized PHA, with half decay of COD, is designated as OHA. The OHA is selected as a benchmark oxidized humic acid for our study, because it shows significantly different molecular features compared to PHA and membrane fouling behaviors. For the mass production of OHA in the following batches of photocatalysis, the PHA solution was irradiated for the pre-determined reaction time of 4.28 h and centrifuged at 13,000 rpm five times, and the supernatant was freeze-dried to obtain the OHA powder. The TiO2 nanoparticles were completely removed from the OHA through the repeated centrifugation, and no Ti signal was observed in XPS for the OHA powder. Details are provided in the Supplementary materials and in Table S1.

## 2.2. Membrane filtration

To explore membrane fouling, the tangential flow filtration experiments were conducted in a flow-through membrane unit. The flow rate of the feed was maintained at  $100\,\mathrm{mL\,min}^{-1}$ , and the concentrate was recirculated back to the reservoir while the filtrate was collected. A membrane was first thoroughly rinsed with ultrapure water, and precompacted with the ultrapure water under 15 psi for 2 h to reach a stable membrane flux, which was calculated from the mass of filtrate as a function of time. After water stabilization, PHA and OHA solutions of the same concentration ( $10\,\mathrm{mg\,L}^{-1}$  as COD) were amended, and the membrane flux was monitored as a function of time. The same concentration of PHA and OHA was selected, because our study focuses on how the changes in humic acid molecular structures after photocatalytic oxidation impact membrane fouling, rather than understanding carbon loss in photocatalytic degradation and its effects on membrane fouling.

### 2.3. SEC

SEC was conducted by using a high-performance liquid chromatography (HPLC) system (LC-20, Shimadzu, Japan) coupled with a photodiode array detector (SPD-M20A), in which the absorption was measured at  $\lambda=254\,\mathrm{nm}$  based on previous studies [48–51]. Two gel columns (TSK-GEL G3000PWXL, TSK-GEL G2500PWXL) and a guard column of the same packing material (TSKguardcollum PWxl-CP) were used for SEC at 40 °C. The mobile phase was a phosphate buffer (prepared from  $0.37\,\mathrm{g\,L^{-1}}$  of  $NaH_2PO_4.2H_2O$ ,  $0.57\,\mathrm{g\,L^{-1}}$  of  $Na_2HPO_4.12H_2O$ , and  $3.55\,\mathrm{g\,L^{-1}}$  of  $Na_2SO_4$ ) maintained at pH 6.8, and the flow rate was  $0.5\,\mathrm{mL\,min^{-1}}$ . The HA solutions (PHA or OHA of  $300\,\mathrm{mg\,L^{-1}}$  as COD) were filtered with a  $0.2\,\mu\mathrm{m}$  polytetrafluoroethylene (PTFE) membrane prior to SEC analyses. Control experiments were conducted by using ultrapure water as the blank sample. Polyethylene glycol (HPLC grade) with a molecular size of 330, 700, 1050, 5250, 10,225, and 30,000 Da was used as standard samples.

### 2.4. Contact angle analysis

The analysis of the hydrophilicity of the membrane surfaces was achieved by measurement of sessile drop contact angles between the baseline of the liquid and the tangent at the liquid boundary. To prepare the uniformly coated humic acid coating layers on the bare membranes, a concentrated humic acid solution (PHA or OHA of 563 mg L<sup>-1</sup> as COD) was repeatedly loaded on the membrane surfaces with low speed spin-coating and drying. The samples were dried for 24 h in a vacuum drying container before performing contact angle measurements. Scanning electron microscopy (SEM) of the bare and humic acid coated membranes revealed that uniform and sufficient coatings were achieved (Fig. S1). Images of ultrapure water droplets on three different membrane surfaces (i.e., a bare membrane, a PHA coated membrane, and an OHA coated membrane) were obtained by a contact angle goniometer equipped with an environmental chamber (Krüss IL4201). For each membrane sample, five sets of equilibrium sessile drop contact angles were recorded between 30 and 60 s after the drop loaded on the membrane surface. In the contact angle analysis, the humic acids are expected to dissolve in the water drops only to a minimal extent due to the very short exposure (less than 60 s), which should not affect the contact angle results.

### 2.5. XPS

The oxidation states and bonding environment of PHA and OHA were characterized by XPS, which was conducted on a PHI 5600 system with a Mg Ka source (1253.6 eV) and under ultrahigh vacuum conditions (pressure  $< 10^{-8}$  Torr). Escaped photoelectrons were captured and analyzed by a hemispherical energy analyzer operating at a constant pass-energy of 58.7 eV. Peak positions were referenced to C1s, at 284.5 eV. The humic acid powder (i.e., freeze-dried PHA or OHA) was used for sample analysis.

## 2.6. Fluorescence EEM spectroscopy

Fluorescence EEM spectroscopy was used to evaluate fluorescent organic substances of PHA and OHA. The humic acid solutions were first filtered through a 0.45  $\mu m$  PVDF membrane, and the fluorescence EEM spectra were recorded using an F-700 spectrofluorometer (Hitachi, Inc., Japan). Fluorescence EEM spectroscopic measurements were performed over an excitation wavelength ranging from 220 to 450 nm with a 5 nm increment and an emission wavelength ranging from 280 to 560 nm with a 1 nm increment. As to the fluorescence EEM analyses, three-dimensional spectra were plotted using MATLAB and Origin. Control experiments were conducted to exclude background fluorescence of the blank sample of ultrapure water.

## 2.7. AFM

The AFM measurements were carried out on an MFP3D-SA microscope and a Cypher S microscope, both from Asylum Research (Santa Barbara, CA, USA). Silicon wafers (Ted Pella, Inc.) used to calibrate the AFM tips were rinsed with isopropyl alcohol, ethanol, and ultrapure water successively before heating them with a butane torch (until bright orange glowing) for 30 s. An Olympus AC200TS cantilever with a fundamental resonance frequency of ca. 137.81 kHz and a fundamental force constant of ca. 7.40 N m<sup>-1</sup> was used for imaging. For imaging purposes, we dried the fouled membranes (from membrane filtration experiments) in vacuum at room temperature for 24 h. For contact resonance force microscopy (CRFM) measurements, we used an Olympus AC240TS cantilever with a fundamental resonance frequency of ca. 242.15 kHz and a fundamental force constant of ca. 1.08 N m<sup>-1</sup>, and applied a static load of 20 nN. To infer the mechanical properties of the humic acids rather than the PVDF support, PVDF membranes were fully coated by PHA or OHA via repeated loading and drying of concentrated humic acid solutions, as described in the contact angle analysis section. CRFM was performed on dried bare membranes and on humic acid coated membranes. To explore the foulant-foulant and foulant-membrane adhesion forces in an aqueous environment, amine group (-NH<sub>3</sub>) functionalized polystyrene microspheres (25 µm in diameter) were coated with PHA or OHA and used as AFM probes to investigate the interaction between PHA and the bare membrane, PHA and the PHA fouled membrane, OHA and the bare membrane, and OHA and the OHA fouled membrane. For the AFM tests, the cantilever was already loaded with an amine functionalized microsphere (commercially available from Novascan Technologies), and PHA or OHA coating was obtained by repeatedly soaking and drying the probes in a drop of 20 µL PHA or OHA solution (160 mg  $L^{-1}$ , pH 7) on the atomic force microscope stage. The mass increase of the cantilever was characterized by the resonance frequency after humic acid coating, and it was verified through calculations that the humic acid should be sufficient to cover the probe. In addition, SEM was used to examine the probe before and after humic acid coating. The results showed that the probe surface became smooth and uniform after coating, which also provided a direct evidence of the successful loading of humic acids onto the probe (Fig. S2). During force measurements, the PHA or OHA coated probes were used to contact a bare or humic acid fouled membrane in the aqueous environment, in which at least 180 force curves for six random spots were obtained for each sample at room temperature. The adhesion force of each force curve was obtained based on the retraction of the PHA or OHA coated probe from the membrane surface. The fundamental force constants for the PHA coated probe and OHA coated probes were ca. 5.41 and 5.37 N m<sup>-1</sup>, respectively, and a tip approaching velocity of 300 nm s<sup>-1</sup> was used for the analyses.

#### 3. Results and discussion

## 3.1. Membrane fouling was less significant by OHA than PHA of the same concentration

Membrane flux, normalized to the initial flux of time zero, for PHA and OHA fouling decreased significantly as a function of time at the beginning of the filtration tests (i.e., 0–5 min) before leveling off (Fig. 1). For the later stage of the filtration tests (i.e., after 5 min), the membrane flux decreased more apparently for OHA than PHA, possibly suggesting that for OHA, the filtration required a longer time to reach to a steady state. For all filtration tests with time duration of 140 min, OHA showed less membrane fouling than PHA; the membrane flux was 21.3% more for the OHA fouling test than for the PHA fouling test at the end of the 140 min filtration period. The PHA and OHA removal in terms of COD after membrane filtration was  $34.7 \pm 1.5\%$  and

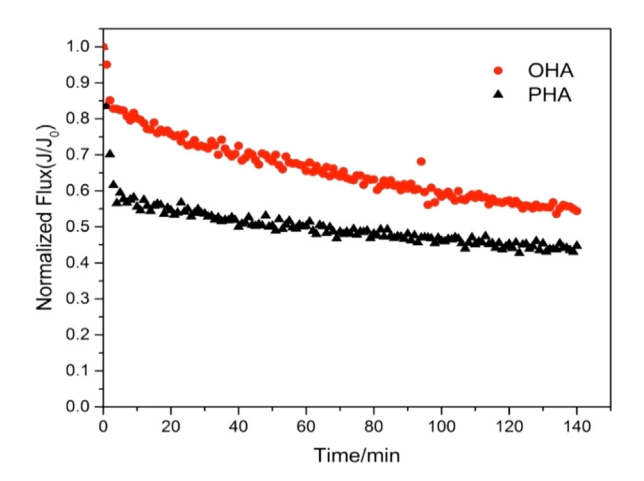


Fig. 1. Membrane flux as a function of time in PHA or OHA fouling experiments.

52.5 ± 0.6%, respectively. Repeated membrane fouling experiments were also conducted, and the results also suggested OHA fouled membrane less than PHA. The results demonstrate that photocatalytic oxidation is a viable process to reduce humic acid fouling of ultrafiltration membranes. Similarly, such an enhanced flux after the photooxidation of humic acid has been reported, and primarily attributed to changes in the molecular characteristics of the humic acids resulting from preferential decomposition of large molecular-size and hydrophobic moieties [52]. Notably, both PHA and OHA of the same concentration (i.e.,  $10 \,\mathrm{mg}\,\mathrm{L}^{-1}$  as COD) were used for the filtration tests, and the results suggested that the changes in humic acid characteristics after photocatalytic oxidation played a critical role for mitigating membrane fouling, rather than the mineralization and mass reduction of the humic acid. To further understand the mechanism of membrane mitigation of humic acid after photocatalysis and to identify the underlying physical, chemical, and mechanical characteristics of the humic acid that determine membrane fouling during photocatalysis, subsequent characterization of PHA and OHA has been performed and discussed.

### 3.2. SEC suggested that OHA had a smaller molecular size than PHA

Size-exclustion chromatography was conducted to determine the molecular weight of PHA and OHA. According to Fig. 2, PHA had a broad molecular size distribution, from 100 Da to 10 kDa, consistent with previously reported data for the same Sigma-Aldrich humic acid [53]. The dominant molecular size was 1281 Da based on UV absorption at 254 nm. After photocatalytic oxidation, OHA also had a broad molecular size distribution, similar to that of PHA; however, the distribution shifted to small molecular sizes, and the most dominant size was 625 Da based on UV absorption at 254 nm. The results might indicate that the large molecular size components of PHA degraded and formed smaller molecular size fractions during photocatalysis, likely due to the depolymerization and mineralization of the humic acid under the attack of •OH [54]. Additionally, OHA still had the residue of large molecular size components (e.g., 3181 Da), which could be due to the presence of recalcitrant moieties in the humic acid in photocatalysis and •OH oxidation. Morover, the PVDF ultrafiltration membranes used in our study had a MWCO of 100 kDa, which is much larger than the moleclar size of the Sigma-Aldrich humic acid. Our findings suggested that the humic acid, irrespective of photocatalytic oxidation, fouled the membranes via adsorption rather than pore blocking. Similar to the

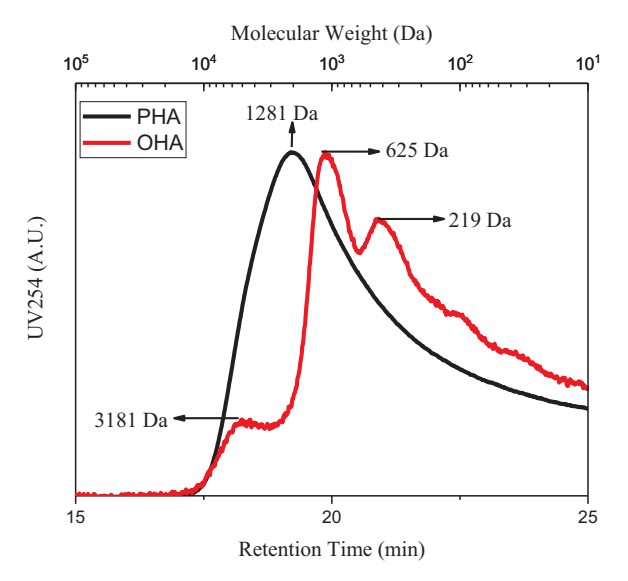


Fig. 2. Molecular size of PHA and OHA. Humic acid was characterized by UV absorption at 254 nm (A.U. represents "arbitrary units").



**Fig. 3.** Sessile drop contact angle profiles on a bare membrane, a PHA coated membrane, and an OHA coated membrane. Data on contact angles are reported as the mean plus/minus the standard deviation.

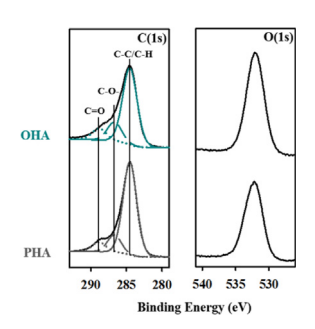
advanced oxidation of photocatalysis, ozone was also used to pretreat the water containing humic acids to mitigate membrane fouling, and the results suggested that the membrane pore size played an important role in fouling [55,56]. Ozone oxidation could reduce the molecular size of the humic acids from larger than the membrane pore size to smaller than the membrane pore size, and the oxidation could change the fouling mechanism from pore blocking to surface adsorption, which might intensify membrane fouling. Photocatalysis could also change the relative relationship between the humic acid molecular size and membrane MWCO, and might increase fouling. Therefore, special attention should be paid to the extent of photocatalytic oxidation of the humic acid for membrane fouling control. To understand the adsorption of the humic acid on membrane surfaces before and after photocatalytic oxidation, the chemical and mechanical properties of the foulants were further characterized.

# 3.3. Contact angle analyses suggested that OHA was slightly more hydrophilic than PHA

Fig. 3 shows that both PHA and OHA coated membranes had a smaller contact angle with water than that of the bare PVDF membrane (85.5  $\pm$  0.6°). The contact angle of the OHA coated membrane was slightly smaller than that of the PHA coated membrane (46.1  $\pm$  0.9° vs. 51.0  $\pm$  1.2°), and hence OHA was more hydrophilic than PHA. For the coated membrane samples, the humic acids sufficiently covered the membrane surface, so the characterized properties represent those of the humic acids. Additionally, the membrane flux during humic acid fouling experiments correlates well with the change of hydrophilicity, which may indicate that a more hydrophilic membrane surface can alleviate the initial absorption of foulant layers on the membrane surface [57]. The humic acid became more hydrophilic after photocatalysis, which could be ascribed to the introduction of hydrophilic functional groups (e.g., -OH, -COOH) into the humic acid by TiO2 treatment [41,58]. Considering the reduction of the molecular size and mass of the humic acid during photocatalysis, we speculate that humic acid oxidation started with the introduction of hydrophilic functional groups and proceeded with depolymerization and mineralization.

## 3.4. XPS suggested OHA had an increased oxygen content compared to PHA

The elemental composition, oxidation state, and bonding environment of PHA and OHA were investigated by XPS (Fig. 4). According to the binding energy, the C1s peaks at 288.0 eV and 286.5 eV corresponded to C=O and C-O bonds, respectively [59]. After photocatalytic oxidation, the peaks representing C=O and C-O increased, which suggested the introduction of oxygen containing functional groups (e.g., -OH, -COOH) into OHA compared to PHA. In addition, no obvious shift of the C1s binding energy was observed before and after photocatalysis, indicating that the chemical states of carbon in the humic acid samples remained the same. The quantitative elemental composition analysis suggested that the atomic ratio of oxygen to carbon (O/C) increased from 0.35 in PHA to 0.45 in OHA after photocatalysis, with an increase in the contribution of both C=O and C-O (i.e., C=O increased from 7.8%



Sample	O/C	C-C (%)	C-O (%)	C=O (%)
PHA	0.35	77.8	14.4	7.8
OHA	0.45	71.6	17.9	10.5

**Fig. 4.** XPS characterization of PHA and OHA. O/C represents the atomic ratio of oxygen to carbon. C-C, C-O, and C=O represent the contribution of carbon in different bonding environments based on the deconvolution of the carbon peak.

to 10.5% and C-O increased from 14.4% to 17.9%). There was no specific selectivity towards C=O or C-O generation in the humic acid, probably due to the non-selective oxidation by  $\cdot$ OH in TiO<sub>2</sub>-based photocatalysis [60,61]. The results of XPS supported those of the contact angle analysis, and they both highlighted structural changes of the humic acid during photocatalysis.

# 3.5. Fluorescence EEM spectroscopy suggested photocatalytic oxidation might convert the humic acid into small molecules

Fluorescence EEM spectroscopy contour plots in Fig. 5 highlighted the fluorescent response of PHA and OHA under photon excitation, and the results could provide insights into the chemical structure and composition of the humic acid before and after photocatalysis. The typical peaks that can be expected within the limits of the fluorescence EEM spectra (i.e., excitation in the range of 220-450 nm and emission in the range of 280-560 nm) were shown. The qualitative analysis of fluorescence EEM spectra focused on component identification, in which the characteristic peaks matching the data from standard samples including both excitation wavelengths and emission wavelengths were obtained. Five fluorescence components were identified, including tyrosine-like compounds (region I) in the range of  $\lambda_{ex}/\lambda_{em}$ = 220-250 nm / 280-330 nm, tryptophan-like compounds (region II) in the range of  $\lambda_{ex}/\lambda_{em}~=220\text{--}250\,\text{nm}~/~330\text{--}380\,\text{nm},$  fulvic acids (region III) in the range of  $\lambda_{ex}/\lambda_{em} = 220-250 \, \text{nm} \, / \, 380-480 \, \text{nm}, \, \text{so-}$ luble microbial products (region IV) in the range of  $\lambda_{ex}/\lambda_{em}$  $= 250-360 \,\mathrm{nm} / 280-380 \,\mathrm{nm}$ , and humic acids (region V) in the range of  $\lambda_{ex}/\lambda_{em} = 250-450 \, nm$  /  $380-560 \, nm$ . The peaks were observed in region V for both PHA and OHA samples, indicating the presence of the humic acids before and after photocatalysis. However, before photocatalysis, PHA only showed a strong fluoresecence peak in the region V, but not in the other regions of I-IV. This characteristic fluorescence signals distribution was in agreement with other studies of the fluorescence analysis of humic acids [62,63]. Interestingly, OHA showed multiple fluoresence peaks in the regions I-III in addition to region V after photocatalytic oxidation. In addition, the fluoresence peak blueshifted in terms of both excitation and emission wavelengths. Based on the peak assignment, it was inferred that some humic acid components with a relatively large molecular size could be decomposed into small molecules during photocatalysis, and the degradation products contributed to fluorescence in the regions I-III.

# 3.6. AFM imaging indicated OHA formed smaller aggregates on the membrane surface than PHA in fouling experiments

AFM topography was evaluated for the bare membrane and humic

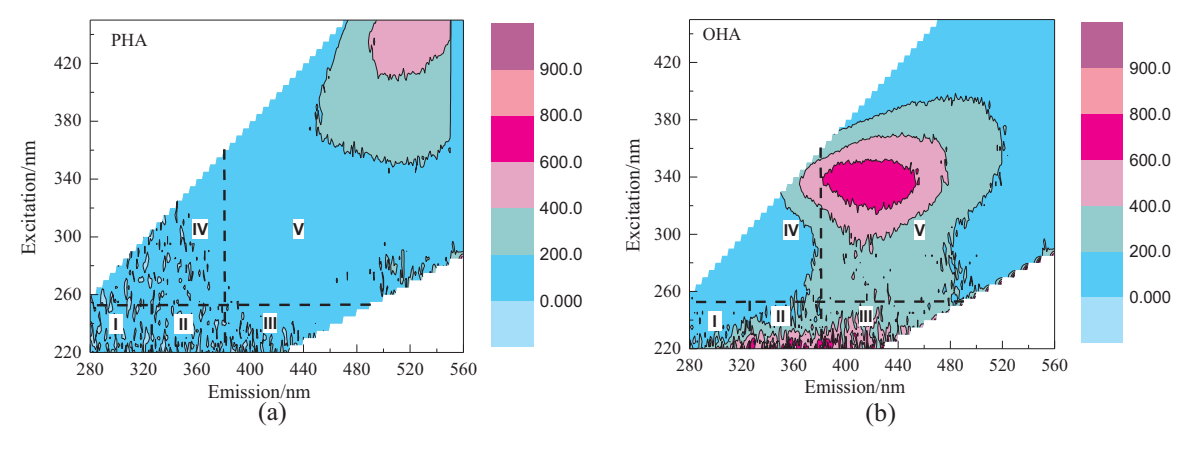


Fig. 5. Fluorescence EEM spectroscopy of (a) PHA and (b) OHA.

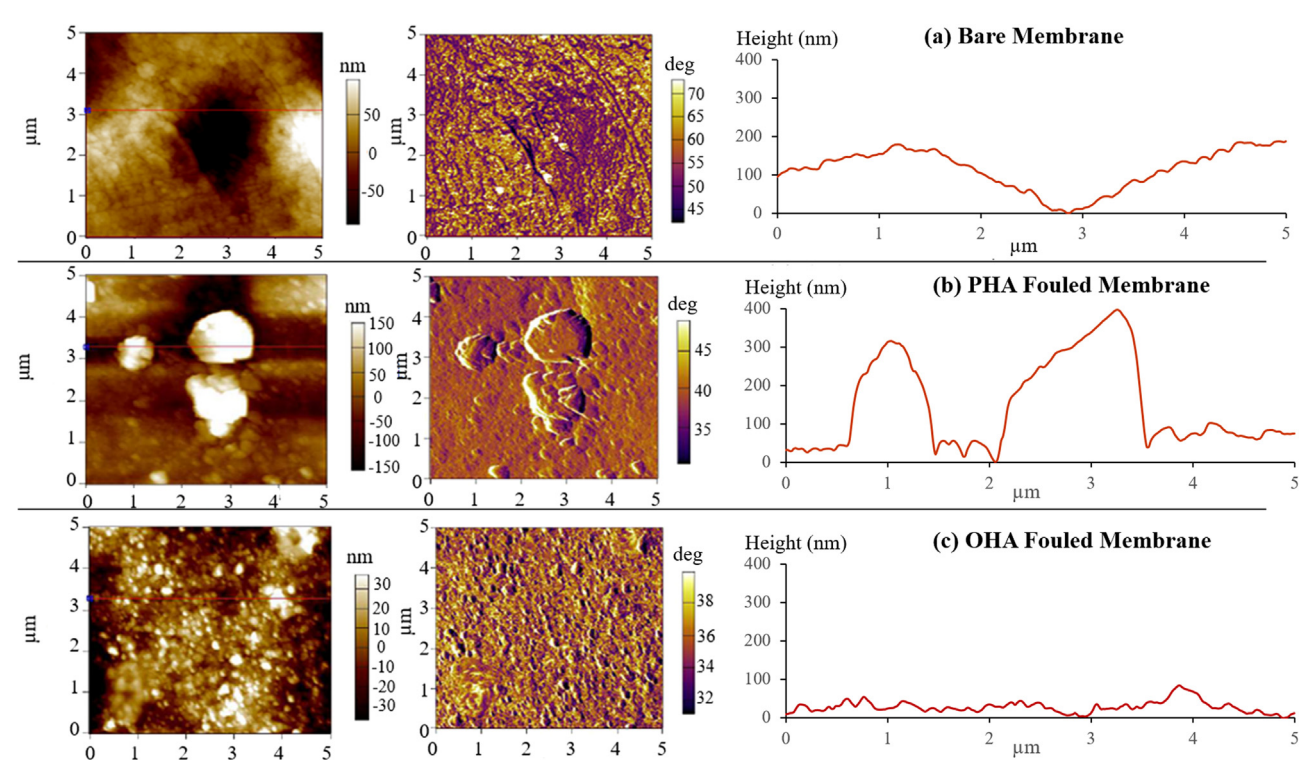


Fig. 6. AFM topography, phase images, and height profiles of (a) a bare membrane (top row), (b) a PHA fouled membrane (middle row), and (c) an OHA fouled membrane (bottom row).

acid fouled membranes, and the height profiles characterized membrane pores, roughness, and foulant aggregates on the membrane surfaces (Fig. 6, left column). Phase imaging was also conducted (Fig. 6, center column), whereby the contrast in the phase images indicates qualitative contrast in the stiffness/softness of the material surface, viscous interactions, and adhesive interactions between the AFM tip and the surface. Phase imaging complements the topography analysis, because it provides insights into the material chemical and mechanical properties beyond height information. For example, the topography of the bare membrane showed a significant height difference (ca. 150 nm) across the imaged area of  $5 \, \mu m$  by  $5 \, \mu m$ ; however, there was little to no variation in the distribution of the contrast features in the phase across the image, due to imaging the same PVDF material across the entire scan area. The range of phase variation is relatively large, but the distribution of features is relatively uniform. In contrast to the bare membrane, the membranes fouled by PHA or OHA showed distinguishable features from the membrane support in the topography and to some extent also in the phase, due to the aggregation of humic acids

on the membrane surface and variations in material properties. The topography clearly indicated that PHA formed larger aggregates on the membrane surface than OHA (lateral size of ca. 0.2-1.3 vs. 0.05-0.2 µm), and the small OHA aggregates were more uniformly distributed on the membrane surface than the large PHA aggregates. The height profiles also suggested that PHA aggregates were higher than OHA aggregates (ca. 270-340 vs. 20-70 nm). Moreover, the PHA fouled membrane exhibited a higher root mean squared (RMS) surface roughness compared to the OHA fouled membrane (56.3-213.7 nm vs. 47.9-73.1 nm at different locations of AFM analyses), also suggesting the formation of large PHA aggregates. Photocatalytic oxidation tailors the molecular structure of the humic acid, which impacts foulant aggregation and dispersion on the membrane surface. Oxidation creates more hydrophilic, oxygen containing functional groups in the humic acid, which might reduce the interactions between humic acid molecules (e.g., London dispersion forces, hydrophobic interactions). Further oxidation of the humic acid leads to depolymerization and mineralization, significantly reducing the molecular size of the humic acid

and also the humic acid interactions with itself. The lower tendency of OHA aggregation on the membrane surface could be the result of reduced adhesion forces between OHA molecules, which is supported by the AFM force analysis presented in the next section.

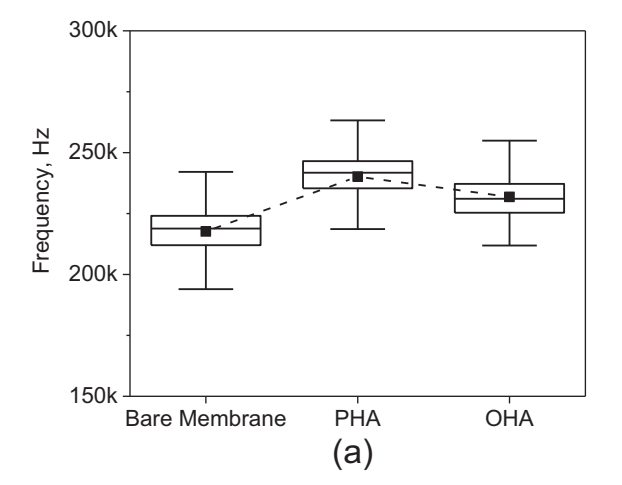
# 3.7. CRFM suggested that OHA was softer and more viscous than PHA under the test conditions

CRFM holds promise for elucidating the inherent mechanical properties of humic acids, i.e., elasticity and viscosity, which provide direct insights into membrane fouling. In CRFM, both the contact resonance frequency and quality factor are recorded, which are related to the stiffness and the energy dissipation of the tip-sample junction during the interaction of the oscillating probe with the material, respectively. An increase in contact resonance frequency corresponds to an increase in sample stiffness, and vice versa; an increase in contact resonance quality factor corresponds to a decrease in viscous dissipation, and vice versa [64,65]. We conducted the CRFM analysis for the bare membrane and PHA and OHA coated membranes, and statistically compared the contact resonance frequency and quality factor of these samples. For the coated membrane samples, the humic acids sufficiently covered the membrane surface, so the characterized properties can represent those of the humic acids. Fig. 7a indicates that the contact resonance frequency increased from the bare membrane to the OHA coated membrane to the PHA coated membrane. The results suggest that the bare membrane is the softest (i.e., lowest elastic modulus), and the humic acids are stiffer (i.e., higher elastic modulus). Moreover, photocatalytic oxidation reduces the stiffness of the humic acid, and hence lower forces are needed to deform OHA than PHA to the same extent. The stiffness of the foulant can be correlated with its fouling potential, because a stiffer foulant may facilitate its stable attachment to the membrane surface [66] and form mechanically strong accumulations to resist mechanical and chemical cleaning. Fig. 7b indicates that the contact resonance quality factor was similar for the bare membrane and the OHA coated membrane, whereas the quality factor was larger for the PHA coated membrane. The results suggest that the bare membrane and OHA exhibit more viscous dissipation than PHA under dynamic testing in the range of 200-260 kHz, used in the CRFM experiments. The foulant that exhibited the highest energy dissipation and loss modulus was obtained after the photocatalytic oxidation. The higher energy dissipation indicates that the OHA foulant is able to undergo a greater degree of irregular and irreversible deformation without disintegration opposed to an elastic body, which recovers its original shape once the deformation forces are removed. This result needs to be interpreted with caution because the viscous dissipation measurement (or the quality factor measurement) in CRFM is dynamic,

and the results are highly dependent on the probing frequency. Increased viscous dissipation of OHA with respect to PHA under a high frequency CRFM measurement cannot necessarily be translated into increased viscous dissipation of OHA with respect to PHA under the conditions typical of membrane filtration (at least not in the same proportion), because a much smaller vibrational frequency is expected for the membrane and the foulant on the membrane surface during filtration or backwashing. In addition, CRFM was conducted for the dried samples to avoid the interference of the water surrounding the AFM probe (AFM measurements in fluid environments are dynamically more complex and often more difficult to interpret quantitatively than in air environments), which may not best characterize the foulant mechanical properties in an aqueous environment. Therefore, adhesion forces were also evaluated subsequently in the aqueous environment to best simulate the scenarios relevant to membrane filtration. Histograms of the contact resonance frequency and quality factor analyses are shown in Fig. S3. The Kolmogorov-Smirnov tests were conducted for the contact resonance frequency and quality factor analyses, and the results showed that any two distributions are statistically different (p < 0.05).

# 3.8. Adhesion force of both foulant-membrane and foulant-foulant decreased after photocatalytic oxidation, as measured by AFM

To investigate the ease of removing the humic acid from the membrane surface or separating the humic acid from itself, adhesion force measurements were performed using static AFM in an aqueous environment. The adhesion force of foulant-membrane decreased after photocatalytic oxidation: the average adhesion force of PHA-membrane and OHA-membrane was 17.6 and 11.2 nN, respectively (Fig. 8). Similarly, the adhesion force of foulant-foulant also decreased after photocatalytic oxidation: the average adhesion force of PHA-PHA and OHA-OHA was 5.4 and 2.0 nN, respectively (Fig. 8). Fig. S4 describing the adhesion force distributions also highlights that low adhesion force dominates after the photocatalytic oxidation of the humic acid. Adhesion forces in the ranges 0-5 or 0-2 nN contributed 51.6% and 76.6% of the force measurements of OHA-membrane and OHA-OHA, in contrast to only 16.3% and 47.2% of the force measurements of PHA-membrane and PHA-PHA. The results suggest that photocatalytic oxidation, which brings about the introduction of hydrophilic, oxygen-containing functional groups and the reduction in the molecular size of the humic acid, reduces the interaction forces between the foulant with the membrane as well as the foulant with itself. We speculate that several mechanisms could lower the adhesion forces, e.g., the reduction of London dispersion forces and hydrophobic interactions, the increase of hydrogen bonding with water, the enhancement of electrostatic repulsion (e.g.,



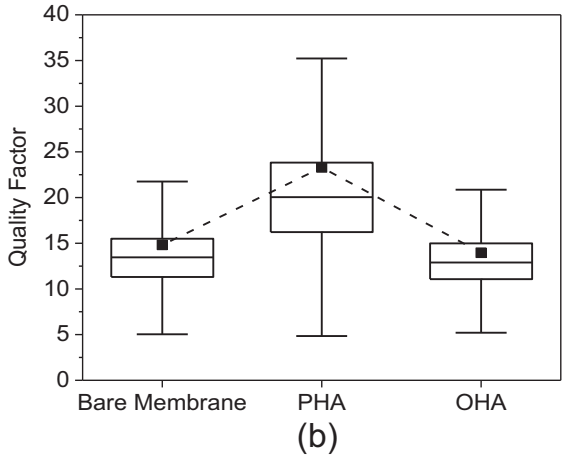


Fig. 7. Contact resonance frequency (a) and quality factor (b) of a bare membrane, a PHA coated membrane, and an OHA coated membrane in the CRFM analysis.

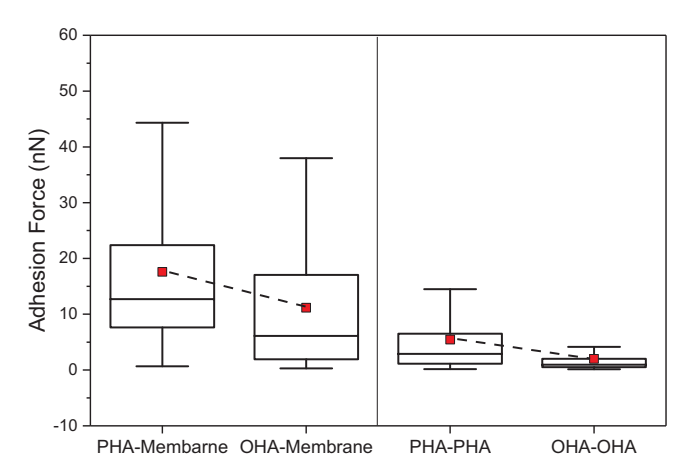


Fig. 8. Adhesion forces of foulant-membrane and foulant-foulant in an aqueous environment.

the presence of more deprotonated -COO groups at circumneutral pH in the fouling tests), changes in geometrical arrangements and constraints, etc., but further research is needed to fully understand the dominant effects. Furthermore, the adhesion force of foulant-foulant was much smaller than that of foulant-membrane. This observation is in agreement with the findings of Wang et al., in which a reduced adhesion force was observed for foulant-foulant with respect to foulant-membrane for the fouling of bovine serum albumin, sodium alginate, a humic acid, and secondary wastewater effluent organic matter for PVDF ultrafiltration membranes [67]. Hence, the reduction of the membranefoulant adhesion force might be important for controlling humic acid fouling of the membranes in our study, and it could be achieved via the surface modification of the membranes and the introduction of hydrophilic functional groups. The Kolmogorov-Smirnov tests were also conducted for the adhesion force analyses, and the results showed that any two distributions were statistically different (p < 0.05).

## 3.9. Mechanism of membrane fouling by humic acids

Photocatalysis introduces oxygen-containing functional groups (e.g., -OH and -COOH) into the humic acid, leading to an increase of hydrophilicity, which was demonstrated by XPS and the contact angle analysis. According to the SEC and fluorescence EEM spectroscopy analysis, PHA with large molecular sizes depolymerized and decomposed into OHA with small molecular sizes. The structural change of the humic acid could reduce the interactions of membrane-foulant and foulant-foulant, which were a key factor controlling membrane fouling. The results support our observations in AFM topography and adhesion force analysis: humic acid reduced aggregate size on the membrane surface, and the adhesion force of membrane-foulant and foulant-foulant decreased. The adhesion forces of membrane-foulant were larger than those of foulant-foulant, irrespective of the humic acid before or after photocatalytic oxidation, which supports the argument that reducing membrane-foulant interactions is critical for membrane fouling control. In Fig. 9, we provide a comprehensive comparison between PHA and OHA in terms of their topographical, physical, chemical, and mechanical properties, and correlate these critical properties to their contribution to membrane fouling in our study. The radar map highlights that photocatalytic oxidation reduces the hydrophobicity, carbon/oxygen atomic ratio, molecular size, aggregate size, and adhesion forces of the humic acid and thus can mitigate membrane fouling.

#### 4. Conclusion

Photocatalytic membrane filtration is promising for water and wastewater treatment, because it combines physical rejection and

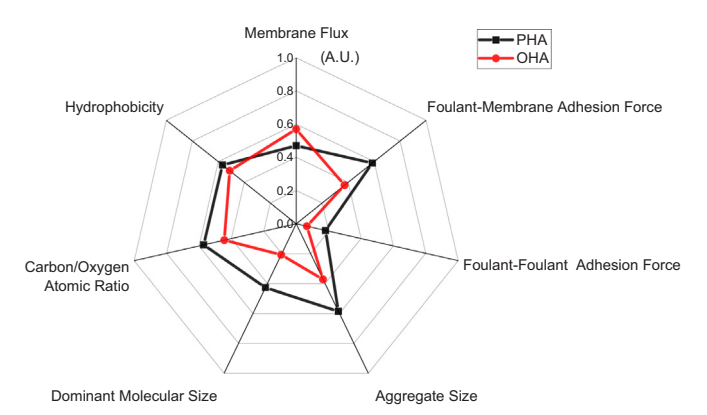


**Fig. 9.** Critical properties of PHA and OHA and their contribution to membrane fouling. The data in the radar map were drawn to scale. The membrane flux was the flux at the end of the filtration process normalized to the initial flux at time zero. The foulant-membrane adhesion force and foulant-foulant adhesion force correspond to the average adhesion force normalized to 30 nN. The aggregate size corresponds to the lateral size of humic acid aggregates on fouled membranes normalized to 2 µm. The molecular size was the most dominant molecular size normalized to 3 kDa. The carbon/oxygen atomic ratio corresponds to the XPS measurements normalized by 5. Hydrophobicity corresponds to the contact angle with water normalized to 90°. A.U. indicates "arbitrary units".

chemical degradation to improve the performance of contaminant removal, it minimizes brine/waste generation and the need for further treatment or disposal, it prevents membrane fouling by oxidizing NOM and biofilms, and it may potentially use renewable solar energy to promote sustainable water purification. Our study gained mechanistic understanding on how the photocatalytic membrane system mitigated membrane fouling from a humic acid, which is model NOM. We first prepared OHA from partial oxidation of PHA in TiO2-based photocatalysis, and then used both humic acids, i.e., PHA and OHA, for the fouling of PVDF ultrafiltration membranes. The results suggested that OHA fouled the membranes to a lesser extent than PHA, whereby the same concentration for the humic acids was used. Next, humic acid properties were systematically evaluated, and it was found that the humic acid exhibited lower molecular weight and increased hydrophilicity and oxygen content after photocatalytic oxidation. Photocatalysis likely introduces oxygen-containing functional groups, e.g., -OH and -COOH, into the molecular structure of the humic acid, and depolymerizes or mineralizes the humic acid to form smaller fragments. Topological characterization of the humic acid on fouled membranes indicated that OHA formed smaller aggregates than PHA, and the adhesion force of both foulant-membrane and foulant-foulant decreased after the photocatalysis of the humic acid. The adhesion forces of membrane-foulant were larger than those of foulant-foulant, irrespective of PHA or OHA, which supports the argument that reducing membrane-foulant interactions is critical for membrane fouling control. CRFM suggested that the humic acid became softer (less stiff) and more viscous after photocatalytic oxidation, although the result cannot be generalized because the measured viscous dissipation was highly dependent on the measurement resonance frequency and the water content of the sample. A radar map was created to compare PHA and OHA in terms of their topographical, physical, chemical, and mechanical properties, and to correlate these critical properties with their contribution to membrane fouling. Our study not only provides mechanistic understanding of humic acid fouling in a photocatalytic membrane system at the molecular level, but also sheds light into the development of new membrane materials and processes to mitigate fouling. Our work can also be useful in the related fields of membrane fouling control, e.g., by ozone or other oxidants, for mitigating membrane fouling of NOM or biofilms.

#### Acknowledgements

We acknowledge National Science Foundation grant CBET-1604886 and a start-up grant from the Department of Civil and Environmental Engineering at The George Washington University (GWU). We thank Prof. Lijie Grace Zhang in the GWU Department of Mechanical and Aerospace Engineering for contact angle analyses. We also thank Qinmin Zheng and Tao Ye in the Department of Civil and Environmental Engineering at GWU for technical assistance and fruitful discussions for this study.

#### Appendix A. Supplementary material

Supplementary data associated with this article can be found in the online version at http://dx.doi.org/10.1016/j.memsci.2018.06.017.

#### References

- [1] B. Van der Bruggen, C. Vandecasteele, T. Van Gestel, W. Doyen, R. Leysen, A review of pressure-driven membrane processes in wastewater treatment and drinking water production, Environ. Prog. Sustain. Energy 22 (2003) 46–56.
- [2] S. Hong, M. Elimelech, Chemical and physical aspects of natural organic matter (NOM) fouling of nanofiltration membranes, J. Membr. Sci. 132 (1997) 159–181.
- [3] E.M. Vrijenhoek, S. Hong, M. Elimelech, Influence of membrane surface properties on initial rate of colloidal fouling of reverse osmosis and nanofiltration membranes, J. Membr. Sci. 188 (2001) 115–128.
- [4] L.F. Greenlee, D.F. Lawler, B.D. Freeman, B. Marrot, P. Moulin, Reverse osmosis desalination: water sources, technology, and today's challenges, Water Res. 43 (2009) 2317–2348.
- [5] F. Meng, F. Yang, B. Shi, H. Zhang, A comprehensive study on membrane fouling in submerged membrane bioreactors operated under different aeration intensities, Sep. Purif. Technol. 59 (2008) 91–100.
- [6] M.A. Shannon, P.W. Bohn, M. Elimelech, J.G. Georgiadis, B.J. Marinas, A.M. Mayes, Science and technology for water purification in the coming decades, Nature 452 (2008) 301.
- [7] W. Yuan, A.L. Zydney, Humic acid fouling during microfiltration, J. Membr. Sci. 157 (1999) 1–12.
- [8] M. Erhayem, M. Sohn, Stability studies for titanium dioxide nanoparticles upon adsorption of Suwannee River humic and fulvic acids and natural organic matter, Sci. Total Environ. 468 (2014) 249–257.
- [9] P.C. Singer, Humic substances as precursors for potentially harmful disinfection byproducts, Water Sci. Technol. 40 (1999) 25–30.
- [10] J. Cho, G. Amy, J. Pellegrino, Membrane filtration of natural organic matter: initial comparison of rejection and flux decline characteristics with ultrafiltration and nanofiltration membranes. Water Res. 33 (1999) 2517–2526.
- [11] C. Combe, E. Molis, P. Lucas, R. Riley, M.M. Clark, The effect of CA membrane properties on adsorptive fouling by humic acid. J. Membr. Sci. 154 (1999) 73–87.
- [12] M. Mänttäri, L. Puro, J. Nuortila-Jokinen, M. Nyström, Fouling effects of polysaccharides and humic acid in nanofiltration, J. Membr. Sci. 165 (2000) 1–17.
- [13] L.D. Nghiem, D. Vogel, S. Khan, Characterising humic acid fouling of nanofiltration membranes using bisphenol A as a molecular indicator, Water Res. 42 (2008) 4049–4058.
- [14] A. Seidel, M. Elimelech, Coupling between chemical and physical interactions in natural organic matter (NOM) fouling of nanofiltration membranes: implications for fouling control, J. Membr. Sci. 203 (2002) 245–255.
- [15] C.Y. Tang, Y.-N. Kwon, J.O. Leckie, Characterization of humic acid fouled reverse osmosis and nanofiltration membranes by transmission electron microscopy and streaming potential measurements, Environ. Sci. Technol. 41 (2007) 942–949.
- [16] S.-H. Yoon, C.-H. Lee, K.-J. Kim, A.G. Fane, Effect of calcium ion on the fouling of nanofilter by humic acid in drinking water production, Water Res. 32 (1998) 2180–2186.
- [17] Z. Yan-jun, W.U. Kai-fen, W. Zheng-jun, Z. Liang, L. Shu-shen, Fouling and cleaning of membrane–a literature review, Environ. Sci. 12 (2000) 241–251.
- [18] Y.-H. Zhao, K.-H. Wee, R. Bai, Highly hydrophilic and low-protein-fouling polypropylene membrane prepared by surface modification with sulfobetaine-based zwitterionic polymer through a combined surface polymerization method, J. Membr. Sci. 362 (2010) 326–333.
- [19] Y. Chang, W.-J. Chang, Y.-J. Shih, T.-C. Wei, G.-H. Hsiue, Zwitterionic sulfobetaine-grafted poly (vinylidene fluoride) membrane with highly effective blood compatibility via atmospheric plasma-induced surface copolymerization, ACS Appl. Mater. Interfaces 3 (2011) 1228–1237.
- [20] G. Kang, Y. Cao, Development of antifouling reverse osmosis membranes for water treatment: a review, Water Res. 46 (2012) 584–600.
- [21] J.G. Jacangelo, J. DeMarco, D.M. Owen, S.J. Randtke, Selected processes for removing NOM: an overview, J. -Am. Water Works Assoc. 87 (1995) 64–77.
- [22] B.S. Karnik, S.H. Davies, K.C. Chen, D.R. Jaglowski, M.J. Baumann, S.J. Masten, Effects of ozonation on the permeate flux of nanocrystalline ceramic membranes, Water Res. 39 (2005) 728–734.
- [23] S. Van Geluwe, L. Braeken, B. Van der Bruggen, Ozone oxidation for the alleviation of membrane fouling by natural organic matter: a review, Water Res. 45 (2011)

- 3551-3570.
- [24] R. Gehr, M. Wagner, P. Veerasubramanian, P. Payment, Disinfection efficiency of peracetic acid, UV and ozone after enhanced primary treatment of municipal wastewater, Water Res. 37 (2003) 4573–4586.
- [25] R. Renaud, V. Lazarova, B. Levine, J. Manem, Water reuse: international report, Water Supply 16 (1998) 285–291.
- [26] H.A. Foster, I.B. Ditta, S. Varghese, A. Steele, Photocatalytic disinfection using titanium dioxide: spectrum and mechanism of antimicrobial activity, Appl. Microbiol. Biotechnol. 90 (2011) 1847–1868.
- [27] X. Qu, J. Brame, Q. Li, P.J. Alvarez, Nanotechnology for a safe and sustainable water supply: enabling integrated water treatment and reuse, Acc. Chem. Res. 46 (2012) 834–843.
- [28] X. Qu, P.J. Alvarez, Q. Li, Applications of nanotechnology in water and wastewater treatment, Water Res. 47 (2013) 3931–3946.
- [29] M.A. Shannon, P.W. Bohn, M. Elimelech, J.G. Georgiadis, B.J. Marinas, A.M. Mayes, Science and technology for water purification in the coming decades, Nature 452 (2008) 301.
- [30] M.N. Chong, B. Jin, C.W. Chow, C. Saint, Recent developments in photocatalytic water treatment technology: a review, Water Res. 44 (2010) 2997–3027.
- [31] R. Molinari, C. Lavorato, P. Argurio, Recent progress of photocatalytic membrane reactors in water treatment and in synthesis of organic compounds. A review, Catal. Today 281 (2017) 144–164.
- [32] S. Leong, A. Razmjou, K. Wang, K. Hapgood, X. Zhang, H. Wang, TiO<sub>2</sub> based photocatalytic membranes: a review, J. Membr. Sci. 472 (2014) 167–184.
- [33] W.P. Kwan, B.M. Voelker, Rates of hydroxyl radical generation and organic compound oxidation in mineral-catalyzed Fenton-like systems, Environ. Sci. Technol. 37 (2003) 1150–1158.
- [34] S. Leong, A. Razmjou, K. Wang, K. Hapgood, X. Zhang, H. Wang, TiO<sub>2</sub> based photocatalytic membranes: a review, J. Membr. Sci. 472 (2014) 167–184.
- [35] A.M. Zaky, B.P. Chaplin, Porous substoichiometric TiO<sub>2</sub> anodes as reactive electrochemical membranes for water treatment, Environ. Sci. Technol. 47 (2013) 6554–6563.
- [36] N.A.A. Hamid, A.F. Ismail, T. Matsuura, A.W. Zularisam, W.J. Lau, E. Yuliwati, M.S. Abdullah, Morphological and separation performance study of polysulfone/ titanium dioxide (PSF/TiO<sub>2</sub>) ultrafiltration membranes for humic acid removal, Desalination 273 (2011) 85–92.
- [37] X. Huang, M. Leal, Q. Li, Degradation of natural organic matter by TiO<sub>2</sub> photo-catalytic oxidation and its effect on fouling of low-pressure membranes, Water Res. 42 (2008) 1142–1150.
- [38] R.K. Joshi, P. Carbone, F.-C. Wang, V.G. Kravets, Y. Su, I.V. Grigorieva, H.A. Wu, A.K. Geim, R.R. Nair, Precise and ultrafast molecular sieving through graphene oxide membranes, Science 343 (2014) 752–754.
- [39] X. Zhang, A.J. Du, P. Lee, D.D. Sun, J.O. Leckie, TiO<sub>2</sub> nanowire membrane for concurrent filtration and photocatalytic oxidation of humic acid in water, J. Membr. Sci. 313 (2008) 44–51.
- [40] C.S. Uyguner, M. Bekbolet, Evaluation of humic acid photocatalytic degradation by UV–vis and fluorescence spectroscopy, Catal. Today 101 (2005) 267–274.
- [41] S. Liu, M. Lim, R. Fabris, C. Chow, K. Chiang, M. Drikas, R. Amal, Removal of humic acid using TiO<sub>2</sub> photocatalytic process-fractionation and molecular weight characterisation studies, Chemosphere 72 (2008) 263–271.
- [42] W.R. Bowen, N. Hilal, R.W. Lovitt, C.J. Wright, Characterisation of membrane surfaces: direct measurement of biological adhesion using an atomic force microscope, J. Membr. Sci. 154 (1999) 205–212.
- [43] W.R. Bowen, T.A. Doneva, J.A.G. Stoton, Protein deposition during cross-flow membrane filtration: AFM studies and flux loss, Colloids Surf. B Biointerfaces 27 (2003) 103–113.
- [44] T. Igarashi, S. Fujinami, T. Nishi, N. Asao, K. Nakajima, Nanorheological mapping of rubbers by atomic force microscopy, Macromolecules 46 (2013) 1916–1922.
- [45] G. Liu, S. Yu, H. Yang, J. Hu, Y. Zhang, B. He, L. Li, Z. Liu, Molecular mechanisms of ultrafiltration membrane fouling in polymer-flooding wastewater treatment: role of ions in polymeric fouling, Environ. Sci. Technol. 50 (2016) 1393–1402.
- [46] S. Hong, M. Elimelech, Chemical and physical aspects of natural organic matter (NOM) fouling of nanofiltration membranes, J. Membr. Sci. 132 (1997) 159–181.
- [47] C.Y. Tang, Y.-N. Kwon, J.O. Leckie, Fouling of reverse osmosis and nanofiltration membranes by humic acid—effects of solution composition and hydrodynamic conditions, J. Membr. Sci. 290 (2007) 86–94.
- [48] L.A.T. Espinoza, E. ter Haseborg, M. Weber, F.H. Frimmel, Investigation of the photocatalytic degradation of brown water natural organic matter by size exclusion chromatography, Appl. Catal. B Environ. 87 (2009) 56–62.
- [49] Y. Li, M. Xu, O.J. Sun, W. Cui, Effects of root and litter exclusion on soil CO<sub>2</sub> efflux and microbial biomass in wet tropical forests, Soil Biol. Biochem. 36 (2004) 2111–2114.
- [50] E. O'Loughlin, Y.-P. Chin, Effect of detector wavelength on the determination of the molecular weight of humic substances by high-pressure size exclusion chromatography, Water Res. 35 (2001) 333–338.
- [51] I.V. Perminova, F.H. Frimmel, A.V. Kudryavtsev, N.A. Kulikova, G. Abbt-Braun, S. Hesse, V.S. Petrosyan, Molecular weight characteristics of humic substances from different environments as determined by size exclusion chromatography and their statistical evaluation, Environ. Sci. Technol. 37 (2003) 2477–2485.
- [52] X. Huang, M. Leal, Q. Li, Degradation of natural organic matter by TiO<sub>2</sub> photocatalytic oxidation and its effect on fouling of low-pressure membranes, Water Res. 42 (2008) 1142–1150.
- [53] J. Song, W. Huang, P. Peng, B. Xiao, Y. Ma, Humic acid molecular weight estimation by high-performance size-exclusion chromatography with ultraviolet absorbance detection and refractive index detection, Soil Sci. Soc. Am. J. 74 (2010) 2013–2020.
- [54] A.L. Linsebigler, G. Lu, J.T. Yates Jr, Photocatalysis on TiO<sub>2</sub> surfaces: principles,

- mechanisms, and selected results, Chem. Rev. 95 (1995) 735-758.
- [55] X. Cheng, H. Liang, A. Ding, F. Qu, S. Shao, B. Liu, H. Wang, D. Wu, G. Li, Effects of pre-ozonation on the ultrafiltration of different natural organic matter (NOM) fractions: membrane fouling mitigation, prediction and mechanism, J. Membr. Sci. 505 (2016) 15–25.
- [56] J. Wu, X. Huang, Use of ozonation to mitigate fouling in a long-term membrane bioreactor, Bioresour. Technol. 101 (2010) 6019–6027.
- [57] N.A. Ochoa, M. Masuelli, J. Marchese, Effect of hydrophilicity on fouling of an emulsified oil wastewater with PVDF/PMMA membranes, J. Membr. Sci. 226 (2003) 203–211.
- [58] S. Liu, M. Lim, R. Fabris, C. Chow, M. Drikas, R. Amal, TiO<sub>2</sub> photocatalysis of natural organic matter in surface water: impact on trihalomethane and haloacetic acid formation potential, Environ. Sci. Technol. 42 (2008) 6218–6223.
- [59] P.-L. Desbene, L. Silly, J.-P. Morizur, M. Delamar, XPS analysis of humic and fulvic acids, Anal. Lett. 19 (1986) 2131–2140.
- [60] M. Stylidi, D.I. Kondarides, X.E. Verykios, Pathways of solar light-induced photocatalytic degradation of azo dyes in aqueous TiO<sub>2</sub> suspensions, Appl. Catal. B Environ. 40 (2003) 271–286.
- [61] Z.-R. Tang, Y. Zhang, Y.-J. Xu, Tuning the optical property and photocatalytic performance of titanate nanotube toward selective oxidation of alcohols under ambient conditions, ACS Appl. Mater. Interfaces 4 (2012) 1512–1520.

- [62] N. Hudson, A. Baker, D. Reynolds, Fluorescence analysis of dissolved organic matter in natural, waste and polluted waters—a review, River Res. Appl. 23 (2007) 631–649.
- [63] S. Valencia, J.M. Marín, G. Restrepo, F.H. Frimmel, Application of excitation-emission fluorescence matrices and UV/Vis absorption to monitoring the photocatalytic degradation of commercial humic acid, Sci. Total Environ. 442 (2013) 207–214.
- [64] R.C. Tung, J.P. Killgore, D.C. Hurley, Liquid contact resonance atomic force microscopy via experimental reconstruction of the hydrodynamic function, J. Appl. Phys. 115 (2014) 224904.
- [65] A.B. Churnside, R.C. Tung, J.P. Killgore, Quantitative contact resonance force microscopy for viscoelastic measurement of soft materials at the solid–liquid interface, Langmuir 31 (2015) 11143–11149.
- [66] A.M. Brzozowska, S. Maassen, R. Goh Zhi Rong, P.I. Benke, C.-S. Lim, E.M. Marzinelli, D. Jańczewski, S.L.-M. Teo, G.J. Vancso, Effect of variations in micropatterns and surface modulus on marine fouling of engineering polymers, ACS Appl. Mater. Interfaces 9 (2017) 17508–17516.
- [67] L. Wang, R. Miao, X. Wang, Y. Lv, X. Meng, Y. Yang, D. Huang, L. Feng, Z. Liu, K. Ju, Fouling behavior of typical organic foulants in polyvinylidene fluoride ultrafiltration membranes: characterization from microforces, Environ. Sci. Technol. 47 (2013) 3708–3714.